

Supporting Information

Synthesis of Nanoporous Graphenes via Decarboxylation

Qiulan Zhou^{†a}, Yaping Ma^{†b}, Xuhang Ma^{†b}, Xiaohu Luo^{a,d}, Shizhao Zheng^c, Yanxia Nan^a, Encai Ou^{*a}, Kedong Wang^{*b}, Weijian Xu^{*a}

^aCollege of Chemistry and Chemical Engineering, Hunan University, Changsha 410082, China

^bDepartment of Physics, Southern University of Science and Technology, Shenzhen, 518005, China

^cGuangdong Key Laboratory of Nano-Micro Material Research, School of Chemical Biology and Biotechnology, Shenzhen Graduate School, Peking University, Shenzhen 518055, China

^dSchool of Chemistry and Chemical Engineering, Qiannan Normal University for Nationalities, Duyun, 558000, China

Section S1: Materials

Sodium hydroxide (NaOH; ≥99% purity) were purchased from Sinopharm Chemical Reagent Co., Ltd. Trimesic acid (TMA) (≥98% purity) and benzene-1,3,5-tris(4-benzoic acid) (BTB) were purchased from Aladdin and HWRK CHEM (Beijing, China), respectively. Solubility of TMA is 26.3 g/L (20 °C). 5 wt% Nafion solution was purchased from Dow Chemical Company. All reagents were used without further purification. Double distilled (DI) water were obtained from water treatment equipment (Dow Chemical Company). The para polyphenylene (PPL) autoclave was purchased from Xi'an Changyi Instrument Factory.

Section S2: Synthesis of NPG-2

In Fig. S1, similar to that of NPG-1, after carboxylic acid dissociates to form carboxyl anion linking with phenyl, the phenyl is obtained through the decarboxylation reaction excited by heating. Finally, the formation of NPG-2 is due to the condensation of the reactive phenyl group.

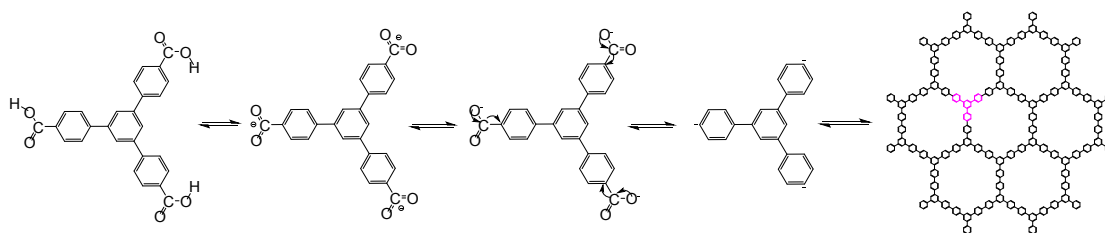


Fig. S1 Possible synthesis process of NPG-2 from BTB and the monomer molecule structure is marked with pink color.

Section S3: Analytical Techniques

Fourier transform infrared (FT-IR) spectra were measured using a Bruker Vertex 70 system.

Catalytic effect of imidazole, triethylamine, ammonia water, and sodium hydroxide for decarboxylation reaction of NPG-1.

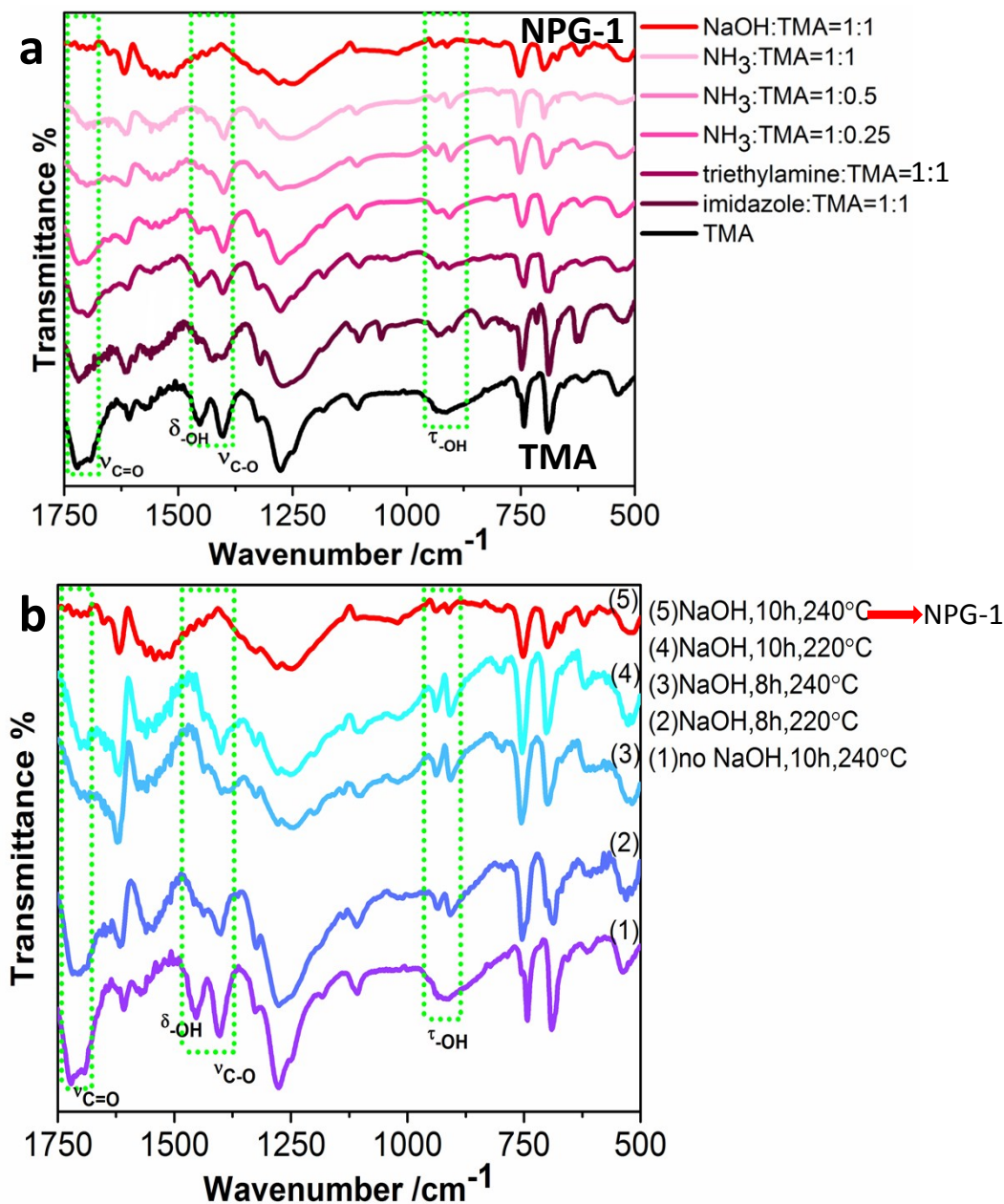


Fig. S2 FT-IR spectra of NPG-1 obtained under different conditions. (a) imidazole, triethylamine, ammonia water and sodium hydroxide, respectively, with TMA at different mole ratio at 10 h and 240°C. (b) $n_{\text{NaOH}}:n_{\text{TMA}} = 1:1$ at different temperature and time.

X-ray photoelectron spectroscopy (XPS) analysis were conducted on an Axis Ultra DLD 600 W instrument (Shimadzu, Japan). The spectrum of O 1s high-resolution XPS

of NPG-1 demonstrates a wide and strong peak at 532.6 eV owing to the organic C-O in NPG-1, which is obviously different from the already reported raw material TMA¹.

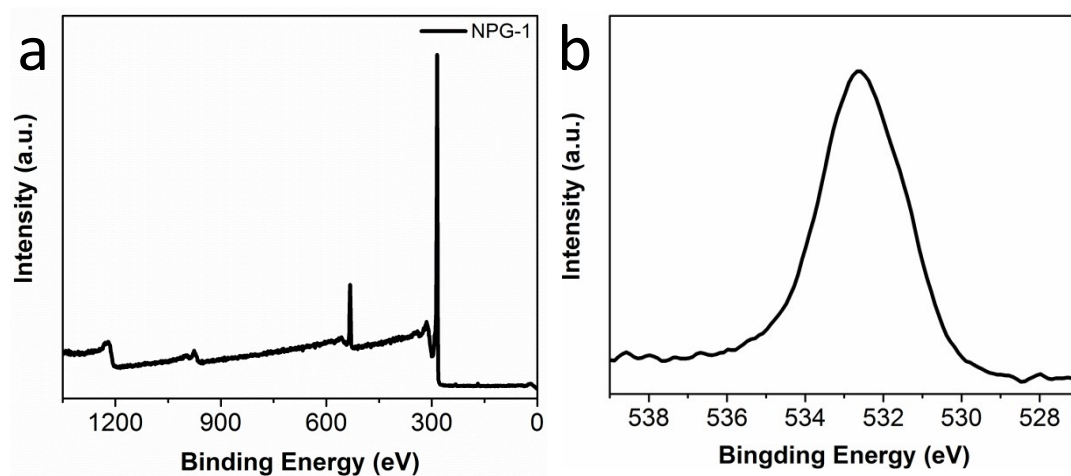


Fig. S3 (a) Survey scan spectrum and (b) O 1s high-resolution XPS of NPG-1.

Table S1. Solubility of NPG-1 in different solvents.

solvent	CH ₃ OH	C ₂ H ₅ OH	CH ₃ OCH ₃	THF	Hex	Toluene	Acetone	MDF	DMSO
NPG-1	NO	NO	NO	NO	NO	NO	NO	NO	partial

The solid-state nuclear magnetic resonance (SSNMR) spectra were collected on a Bruker AV-500NMR spectrometer using a stand Bruker magic angle spinning (MAS) probe with 4-mm (o.d.) zirconia rotors. The magic angle was adjusted by minimizing the number and amplitudes of the signals of the rotational echoes observed in the ⁷⁹Br MAS FID signal from KBr. High power two-pulse phase modulation (TPPM) ¹H decoupling was applied during data acquisition. The decoupling frequency correspond to 32 kHz. The MAS sample spinning rates varied from 8 to 13.5 kHz.

Recycle delays between scans were 2 s. The three undivided broad peaks at 32.46, 7.76 and -13.16 ppm not only verify the spin-induced splitting of adjacent and remote proton of Ar-H², but also confirm the good chemical stability of NPG-1 under high temperature hydrothermal condition.

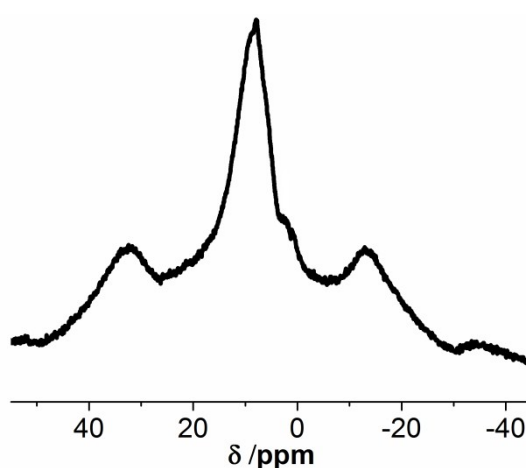


Fig. S4 Solid-state ¹H CP/MAS NMR spectroscopy

X-ray diffraction (XRD) was carried out by the using of a D8 Advance X-ray diffractometer with Cu K α radiation ($\lambda=0.15418$ nm, Bruker, Germany), and the films for XRD characterization were placed on a quartz slide. The structure models of NPG-1 and NPG-2 were built in VESTA software and the theoretical XRD spectra were obtained from the models in Diamond software.

Scanning electron microscopy (SEM, Hitachi S-4800) was performed to study the morphology.

Transmission electron microscopy (TEM) images were obtained with a JEM-3010.

The samples were dispersed in DMF and ultrasonicated for 3 h at 25 °C.

In the thermogravimetric analysis (TGA), the samples were heated from room temperature to 100 °C at a given heating rate same as from 100 to 900 °C. Then, the samples were kept at 100 °C for 30 min to completely remove moisture in the samples and provide a basis for analysis. TGA were carried using a Perkin-Elmer thermal gravimetric analyzer 7 by heating samples in a platinum pan from room temperature 100 °C to 900 °C under nitrogen atmosphere at a heating rate of 5 °C min⁻¹ without an equilibration delay.

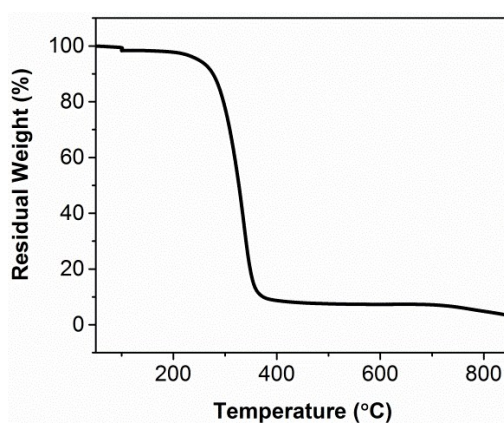


Fig. S5 Thermogravimetric analysis of NPG-1.

Scanning tunneling microscopy (STM) experiments were conducted on a variable temperature system from Scienta Omicron GmbH. Mechanically cut Pt/Ir tips (90% Pt, 10% Ir) were used for topographic measurements. The STM images were analyzed with the WSxM software. The drift of the STM images were corrected by using a procedure proposed by Rahe et al³. The STM samples were prepared by thermal evaporating and depositing the NPGs onto an Au(111) substrate. Before deposition, the Au(111) substrate was cleaned by repeated cycles of Ar⁺ sputtering

(1 kV) followed with annealing at 700 K for three times. NPG-1 powder was loaded into the preparation chamber in a quartz crucible. It was then degassed for 24 hours at $\sim 373\text{K}$. During the deposition, the temperature of NPG-1 was raised to $\sim 411\text{K}$, while the Au(111) substrate was kept at room temperature (300 K). After 1 minute of deposition, the sample was transferred to the STM chamber for testing. The STM measurements were carried out using constant-current mode at room temperature. The base pressure of the preparation chamber and the STM chamber are both below 2×10^{-10} mbar. The preparation procedure of NPG-2 sample is similar, except that a higher temperature of 450K was used during the evaporation and deposition procedure.

Diffuse reflectance UV-Vis spectroscopy was measured on a UV-VISNIR spectrophotometer (UV-3600, Shimadzu Japan). Optical band gap can be obtained according to Tauc Plot method: $(\alpha h\nu)^{1/n} = A(h\nu - E_g)$, in which α , h , ν , A , n , and E_g present the absorbance, Planck constant, frequency, constant, 1/2 or 2 and band gap of semiconductor, respectively. It is speculated that the optical band gap of NPG-1 is 2.86 eV with the $n = 2$.

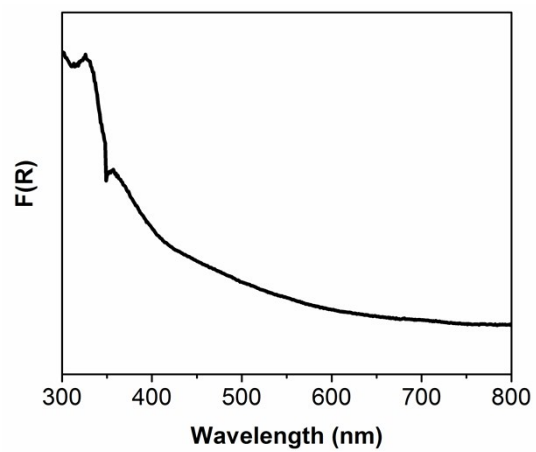


Fig. S6 Solid UV-vis absorption spectrum of NPG-1.

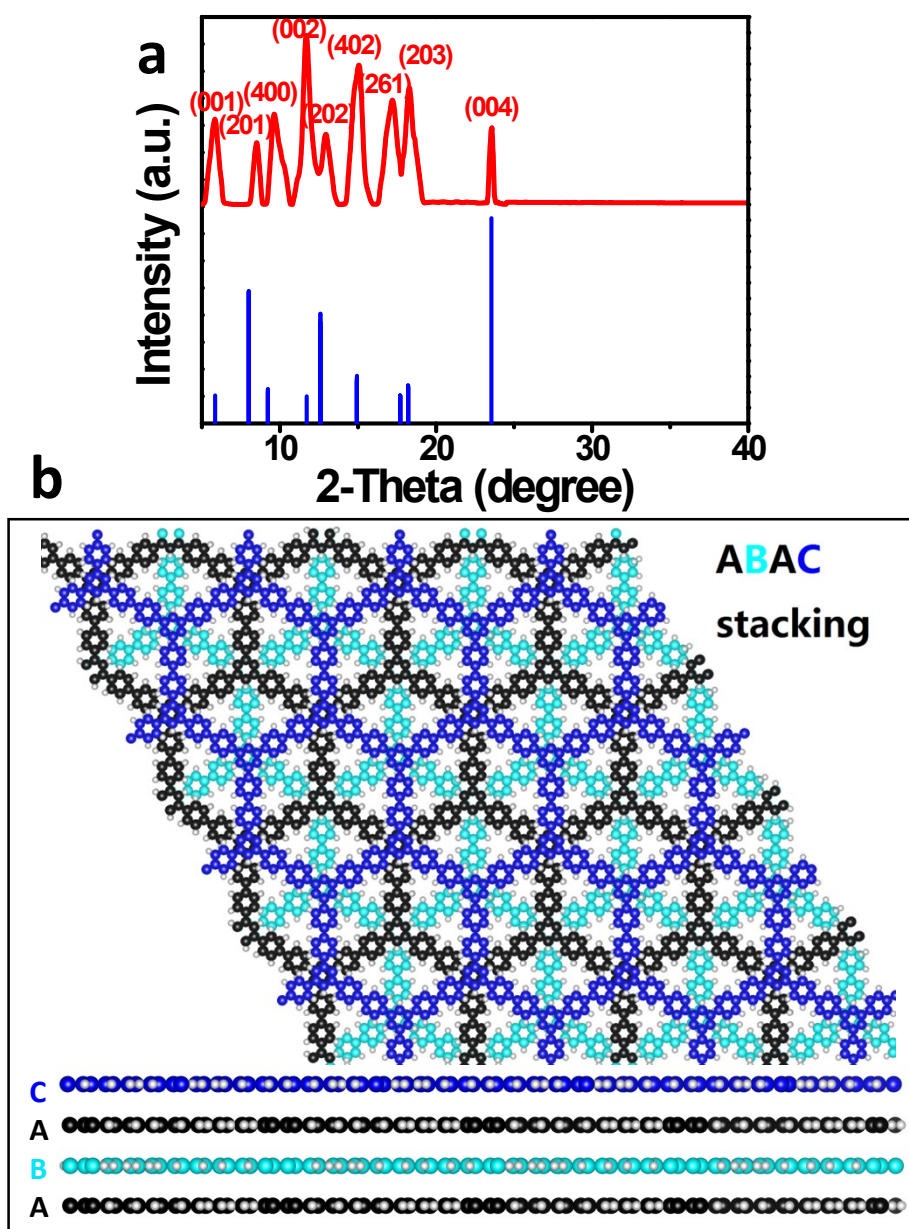


Fig. S7 (a) Experimental (red) and theoretical (blue) XRD patterns, (b) simulated structure with ABAC stacking modes of NPG-2.

As shown in Fig. S8 a Roman numerals (I, II, III, and IV) are used to mark the different chemical states of carbon element of NPG-2. The corresponding HRXPS (Fig. S8 b) of C 1s subpeaks at (I) 285.6, (II)285.1, (III)284.7, and (IV)284.4 eV. The subpeak of “V” at 286.5 eV means the C-O bond, which is the same with NPG-1. Moreover, the area

ratio of four main subpeaks is I: II: III: IV = 1:2:4:1.

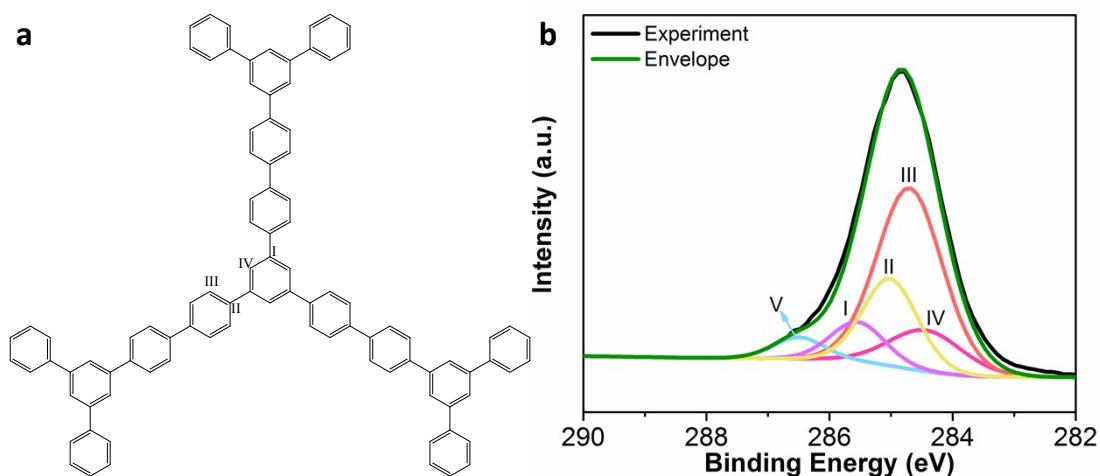


Fig. S8 (a) Partial molecular structure and (b) High-resolution XPS spectrum of C 1s of NPG-2.

Section S3: OER electrocatalytic performance conditions

The electrochemical measures were performed on a CHI 660E electrochemical workstation (Shanghai Chenhua). The three-electrode system consist of glassy carbon electrode (GCE, $d = 3$ mm) as the working electrode, graphite rod electrode as the counter electrode, saturated Ag/AgCl/KCl electrode as the reference electrode and 0.1 M KOH solution as the electrolyte. Same as other work standards, 4 mg catalyst was dispersed in 480 μ L H₂O and 500 μ L CH₃CH₂OH containing 20 μ L 5 wt% Nafion solution by ultrasound to acquire a homogeneous emulsion. Afterwards, 5 μ L catalysts ink were covered on the GCE and then dried at room temperature naturally for measurements. The current density was unified by the geometrical area and the electrode potentials measured (versus Ag/AgCl) were standardized to a reversible hydrogen electrode (RHE) according to the equation: $E_{RHE} = E_{Ag/AgCl} + 0.197 \text{ V} + 0.059 \text{ pH}$. All polarization curves in this work were not rectified by the ohmic potential drop (iR) correction. 5 mV s⁻¹ was used as the scan rate of the linear sweep voltammetry (LSV) measurements.

The linear region was clearly observed on the Tafel plot and its analysis

according to the Tafel equation ($\eta = b \log j + a$, where η is overpotential, j is the current density, and b is the Tafel slope).

The catalyst durability tests were performed in the potential limit from 1.0 to 1.8 V by cyclic voltammogram (CV) at 10 mV/s for 3000 cycles. To evaluate the electrochemical stability of the samples, the time-dependent current density (i-t) curve for NPG-1 and NPG-2 at 1.75 V.

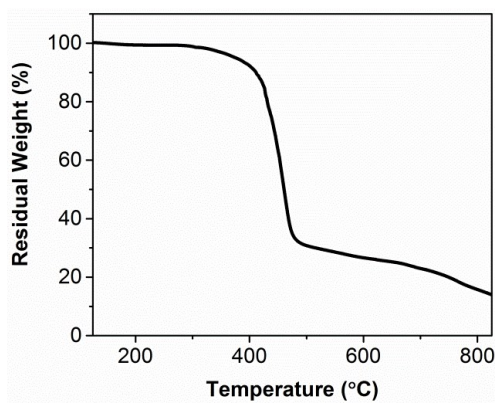


Fig. S9 Thermogravimetric analysis of NPG-2.

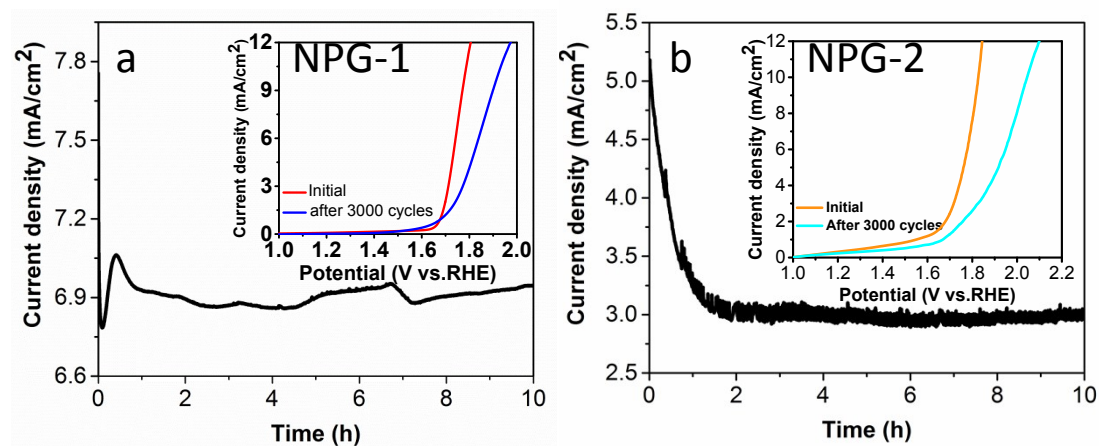


Fig. S10 i-t curve at 1.75 V in 0.1 M KOH media (insert: LSV polarization curves of NPG-1 before and after 3000 cycles) of (a) NPG-1 and (b) NPG-2.

Table S2 Comparison of OER performances between NPG-1, NPG-2, and other graphene electrocatalysts reported previously.

Catalyst	η_{10} (mV vs 1.23 V)	Tafel Slope (Electrolyte	Referenc
----------	----------------------------	---------------	-------------	----------

		mV dec ⁻¹)		e
NPG-1	549	104.6	0.1M KOH	This work
NPG-2	618	210.4	0.1M KOH	
B-N dual-doped porous carbon	570	201	0.1M KOH	[⁴]
pyridinic-N-doped graphene	450	132	1M KOH	[⁵]
pure carbon cloth	570	135.6	1M KOH	[⁶]
NCNF-1000	620	274	0.1M KOH	[⁷]
NPMC-1100	630	104	0.1M KOH	[⁸]

1. T. Classen, M. Lingenfelder, Y. L. Wang, R. Chopra, C. Virojanadara, U. Starke, G. Costantini, G. Fratesi, S. Fabris, S. Gironcoli, S. Baroni, S. Haq, R. Raval and K. Kern, *J Phys Chem A*, 2007, **111**, 12589-12603.
2. P. Horcajada, C. Serre, M. Vallet-Regi, M. Sebban, F. Taulelle and G. Ferey, *Angew Chem Int Ed Engl*, 2006, **45**, 5974-5978.
3. P. Rahe, R. Bechstein and A. Kühnle, *J Vac Sci Technol B*, 2010, **28**, C4E31-C34E38.
4. Y. H. Qian, Z. G. Hu, X. M. Ge, S. L. Yang, Y. W. Peng, Z. X. Kang, Z. L. Liu, J. Y. Lee and D. Zhao, *Carbon*, 2017, **111**, 641-650.
5. Q. C. Wang, Y. J. Ji, Y. P. Lei, Y. B. Wang, Y. D. Wang, Y. Y. Li and S. Y. Wang, *ACS Energy Lett*, 2018, **3**, 1183-1191.
6. Q. Hu, G. M. Li, X. F. Liu, B. Zhu, X. Y. Chai, Q. L. Zhang, J. H. Liu and C. X. He, *Angew Chem Int Ed Engl*, 2019, **58**, 4318-4322.
7. Q. Liu, Y. B. Wang, L. M. Dai and J. N. Yao, *Adv Mater*, 2016, **28**, 3000-3006.
8. J. Zhang, Z. Zhao, Z. Xia and L. Dai, *Nat Nanotechnol*, 2015, **10**, 444-452.